



HAL
open science

Characterization of the Tyranno SA4 third generation SiC fiber surface and comparison with Tyranno SA3 and HNS fibers

James Braun, Clémentine Fellah, Christine Labrugère, Mélanie Vaudescal,
Cédric Sauder

► To cite this version:

James Braun, Clémentine Fellah, Christine Labrugère, Mélanie Vaudescal, Cédric Sauder. Characterization of the Tyranno SA4 third generation SiC fiber surface and comparison with Tyranno SA3 and HNS fibers. *International Journal of Applied Ceramic Technology*, 2024, 10.1111/ijac.14988 . hal-04830435

HAL Id: hal-04830435

<https://hal.science/hal-04830435v1>

Submitted on 12 Dec 2024

HAL is a multi-disciplinary open access archive for the deposit and dissemination of scientific research documents, whether they are published or not. The documents may come from teaching and research institutions in France or abroad, or from public or private research centers.

L'archive ouverte pluridisciplinaire **HAL**, est destinée au dépôt et à la diffusion de documents scientifiques de niveau recherche, publiés ou non, émanant des établissements d'enseignement et de recherche français ou étrangers, des laboratoires publics ou privés.



Distributed under a Creative Commons Attribution - NonCommercial - NoDerivatives 4.0 International License

RESEARCH ARTICLE

Characterization of the Tyranno SA4 third generation SiC fiber surface and comparison with Tyranno SA3 and HNS fibers

James Braun¹  | Clémentine Fellah² | Christine Labrugère³ |
Mélanie Vaudescal³  | Cédric Sauder⁴

¹CEA, DAM, Le RIPAUT, Monts, France

²Université de Lyon, Univ Lyon 1, CNRS UMR5276, ENS de Lyon, Villeurbanne, France

³Univ. Bordeaux, CNRS, PLACAMAT, Pessac, France

⁴Université Paris-Saclay, CEA, Service de recherche sur les matériaux et procédés avancés, Gif-Sur-Yvette, France

Correspondence

James Braun, CEA, DAM, Le RIPAUT, F-37260, Monts, France.

Email: braun@lcts.u-bordeaux.fr

Funding information

Commissariat à l'Énergie Atomique et aux Énergies Alternatives

Abstract

While presenting similar properties, the Hi-Nicalon Type S (HNS) and Tyranno SA3 (TSA3) SiC fibers exhibit different mechanical behaviors when used as reinforcement in SiC/SiC composites. Indeed, the HNS-reinforced composites exhibit a pseudoductile mechanical behavior whereas the TSA3-based composites show low ductility. Even though the differences in their grain size and surface roughness could explain a part of this phenomenon, the chemical composition and microstructure of the fibers outermost surface play a key role. The recent availability of the new Tyranno SA4 (TSA4) SiC fiber allowed the processing of composites showing the expected pseudoductile mechanical behavior in ceramic matrix composites, even without an interphase. Therefore, this result shows that the TSA4 surface should be different from its predecessors. In order to characterize the surface, X-ray photoelectron spectroscopy (XPS), auger electron spectroscopy (AES), and transmission electron microscopy (TEM) were performed on the HNS, TSA3, and TSA4 fibers. The presence of an organized boron nitride layer of dozens of nanometers in thickness on the TSA4 fiber surface was evidenced. This layer already acts as an interphase material, guaranteeing cracks deflection, and is responsible for the pseudoductile behavior of composites made of this new fiber, reducing the interfacial shear stress at the fiber/matrix interface.

KEYWORDS

AES, chemical analysis, SiC fibers, TEM, XPS

1 | INTRODUCTION

Silicon carbide fibers-reinforced silicon carbide matrix composites, referred as SiC/SiC, show outstanding properties at high temperature under oxidative atmosphere,^{1,2} arousing interest for a wide range of high value-added

applications, such as the flight^{3,4} or nuclear industries.^{5–7} It took several decades but the development of nearly stoichiometric SiC fibers, referred as third generation fibers, allowed an increase in their thermal stability as well as their thermomechanical behavior under harsh environments.⁸ Two main third generation commercial

This is an open access article under the terms of the [Creative Commons Attribution-NonCommercial](https://creativecommons.org/licenses/by-nc/4.0/) License, which permits use, distribution and reproduction in any medium, provided the original work is properly cited and is not used for commercial purposes.

© 2024 The Author(s). *International Journal of Applied Ceramic Technology* published by Wiley Periodicals LLC on behalf of American Ceramics Society.

TABLE 1 Main properties of the different third generation SiC fibers (suppliers data).

Fiber	Hi-Nicalon Type S	Tyranno SA3	Tyranno SA4
Type	539341	SA3-S1F08PX	SA4-8PW
Filament/yarn	500	800	800
Mean diameter (μm)	13	10	10
Sizing agent	Polyvinyl alcohol (PVA)	Polyethylene oxide (PEO)	PEO + wax
Sizing content (wt%)	0.9	0.59	0.78
Tensile strength at room temperature (GPa)	3.2	2.24	3.08
Elastic modulus at room temperature (GPa)	371	368	399
TEX (g/km)	198	175	176
Density (g/cm^3)	3.02	3.1	3.09
Thermal conductivity at 25°C (W/m/K)	18	45	45

fibers have widely been studied in the last decades: the Hi-Nicalon Type S (HNS) and the Tyranno SA3 (TSA3). Their main properties are summarized in Table 1. Both fibers exhibit advantages and drawbacks. The TSA3 grain size is larger, leading to higher thermal conductivity⁹ and better thermal stability after annealing at high temperature.¹⁰ The carbon content of the TSA3 fiber at the core is relatively high, in comparison with the HNS one.^{11,12} However, HNS fiber exhibits a better creep behavior under inert atmosphere.^{13,14} The main drawback of the TSA3 fibers lies in the too strong bonding with the SiC matrix in SiC/SiC composite, leading to materials with low damage tolerance.^{15,16} These discrepancies in mechanical behavior, aside from the effect of higher surface roughness,¹² are attributed to difference in the morphology and chemical composition of the fibers outermost surface.¹⁵ To solve this issue, a successor of the TSA3 fiber has been developed, named Tyranno SA4 (TSA4).

An improvement of the mechanical properties (ultimate tensile strength and Young's modulus) has been observed on the TSA4 fiber (Table 1) and could come from the application of previous solutions to reduce abnormal SiC grain growth and free carbon in SA3.¹⁷ However, the thermal conductivity did not change. Recently, mechanical tests conducted on TSA4-based composites with the same interphase and matrix materials as TSA3 ones have highlighted pseudoductile mechanical behavior and equivalent ultimate tensile strength than HNS-based composites.¹⁸ A clear influence of the interphase thickness on the Young's modulus was also observed. This improvement suggests a strong effect of the fibers outermost surface on the mechanical properties.

Indeed, the composition of the fibers surface has been identified as one of the key factor to obtain the expected bonding between the fiber and the matrix in carbon fibers-based polymers,^{19,20} C/C,²¹ or C/SiC.²² Chemical treatments can be employed to modify the fibers surface chemical composition to achieve the fiber/interphase

or fiber/matrix optimal bonding strength.^{23,24} In order to characterize the fibers surface, X-ray photoelectron spectrometry (XPS) was employed either on sized or unsized fibers,^{25,26} as well as auger electron spectroscopy (AES).^{27,28} Raman spectroscopy can also determine the Polyacrylonitrile- or pitch-based carbon fibers microstructure²⁹ and mechanical properties.³⁰ Lately, the interfaces between fibers, interphases, and the matrix have also been characterized through the emergence of new techniques, such as the focused ion beam (FIB), which can be combined with in situ mechanical tests in a scanning electron microscope (SEM).³¹

Therefore, XPS, AES as well as transmission electron microscopy (TEM) were employed to assess the chemical composition and microstructure of the HNS, TSA3, and TSA4 fibers surface. Since the HNS and TSA3 fibers have already been extensively studied,^{8,12,28} the same fiber batches used for manufacturing the composites in ref.,¹⁵ describing the interfaces and interphase microstructures in HNS- and TSA3-based composites and their effect on the macroscopic mechanical behavior, are investigated in the present study. As far as the TSA4 fibers are concerned, the same fiber lot than in ref.¹⁸ was characterized.

2 | MATERIALS AND METHODS

HNS fibers were provided by NGS Advanced Fibers Co., Ltd and TSA3 and TSA4 fibers by UBE Corporation, respectively. The sizing agent of the HNS fibers corresponds to polyvinyl alcohol (PVA) and polyethylene oxide (PEO) for TSA3 and TSA4 fibers. In addition, wax is added on the TSA4. Before the fiber surface analyses, the samples sizing was removed by heat treatment at 900°C under reducing atmosphere (H_2) for 1 h. Previous studies showed that the mechanical properties, microstructure, and grain size do not evolve after similar heat treatments.^{10,13} The chemical composition of HNS, TSA3, and TSA4 fibers was

measured by glow discharge mass spectrometry (GDMS; Astrum GD-MS, Nu Instruments) and instrumental gas analysis (IGA), with LECO CS844 instrument for C and S elements and LECO ONH836 instrument for O, N, and H elements analyses, respectively. Several tows, constituted of hundreds of fibers, of dozens of centimeters were analyzed to reduce the uncertainties.

A K-Alpha ThermoFisher Scientific XPS spectrometer was used with a 1486.6 eV monochromatized Al source and a 200 μm X-ray spot size to determine the fibers outermost surface chemical composition. Initially, full spectra (0–1150 eV) were collected with constant pass energy of 200 eV, while high-resolution spectra (i.e., C1s, O1s, Si2p, B1s, and N1s) were recorded with a constant pass energy of 40 eV. Quantification and fitting were reached with the AVANTAGE software from ThermoFisher Scientific.

A PHI 710 Scanning Auger Nanoprobe equipped with a cylindrical mirror analyzer (CMA) coaxially mounted with respect to the electron column was used to conduct the AES measurements on the fibers. Thanks to this particular system geometry, the take-off angle of the analyzed Auger electrons is below 30° from the primary electron beam and thus permits to avoid shadowing effects. The primary electron beam voltage and current were set at 10 kV and 10 nA to obtain an approximately 20 nm diameter spot size, respectively. Specific areas of a few micron-square were selected for scanning and spectra acquisition in order to optimize the signal-to-noise ratio and limit the charging phenomenon of the surface. Measurement was conducted on a dozen of each fibers. Spectra were acquired in direct mode with a step of 2 eV. The C, O, N, B, and Si KLL peaks were considered. Spectra fitting was performed with MultiPak software using a Shirley-type background subtraction.

Ar⁺ ion etching was employed during both the XPS and AES analyses to determine the fibers in-depth chemical composition (≈ 800 nm and 60 nm maximum depths, respectively). The ion gun was set at 2 kV acceleration voltage and 1 μA current on a 1×1 mm² surface. The sputtered depth was calibrated on SiO₂ substrate prior to the measurements. The change in the peaks intensities was reported as a function of the equivalent sputtered depth in SiO₂.

TEM was also utilized to characterize the fibers surface. A detailed analysis of the HNS and TSA3 fibers can be found in ref.¹⁵ where carbon (002) lattice fringe images were recorded to analyze the structural organization of the carbon-rich surfaces on these fibers. HNS and TSA3 fibers were thinned by FIB (Zeiss Auriga 40) and TSA4 fibers by Gatan precision ion polishing system (PIPS) II. PIPS etching was conducted at 5 keV and finished at 0.5 keV in the fibers longitudinal direction. Thin foils of TSA4 fibers were

TABLE 2 Chemical composition of each fiber from glow discharge mass spectrometry (GDMS) and instrumental gas analysis (IGA; C, N, S, O, and H elements) analyses given in ppm wt, except if mentioned in wt%.

Element	HNS	TSA3	TSA4
H	<10	<10	<10
B	0.24	≈ 0.15 wt%	≈ 0.56 wt%
C	32 wt%	33 wt%	33 wt%
N	110	440	3200
O	4500	360	62
F	≈ 0.31	<0.1	<0.1
Na	6.6	5.5	2.0
Mg	0.62	0.68	2.6
Al	2.9	≈ 0.21 wt%	≈ 0.25 wt%
Si	Matrix	Matrix	Matrix
P	0.98	5.2	3.5
S	45	41	10
Cl	70	5.1	1.8
Ca	45	59	52
Ti	0.41	65	2.4
Cr	<0.3	1.0	0.9
Fe	3.1	14	1.6
Ni	0.51	0.24	0.66
Cu	<0.05	0.17	0.18
Zr	<0.05	7.6	0.2
Hf	<0.05	0.12	<0.05

Abbreviations: HNS, Hi-Nicalon Type S; TSA3, Tyranno SA3; TSA4, Tyranno SA4.

also prepared by FIB (Zeiss NVision 40) to identify and get rid of artifacts due to preparation techniques during TEM analysis.³² Unlike PIPS, FIB also allows to extract samples in the transverse direction of the fibers. A 10 nm gold and a tungsten layers were deposited by sputtering on the fibers surface to limit charging effects and to protect them from the gallium etching ions, respectively. A 30 kV tension and 13 nA intensity were set to take a $20 \times 20 \times 2$ μm^3 cross-section of the fibers. The current was successively reduced from 700 pA to 10 pA to reach a thickness below 100 nm. The HNS and TSA3 fiber surfaces were investigated by a FEI Tecnai F20 ST TEM and TSA4 by a JEOL 2010 F TEM, both operating at 200 kV.

3 | RESULTS AND DISCUSSION

3.1 | Bulk chemical composition

Chemical composition of the fibers assessed from GDMS and IGA (C, N, S, O, and H elements) analyses are presented in Table 2. The TSA4 fiber still contains aluminum,

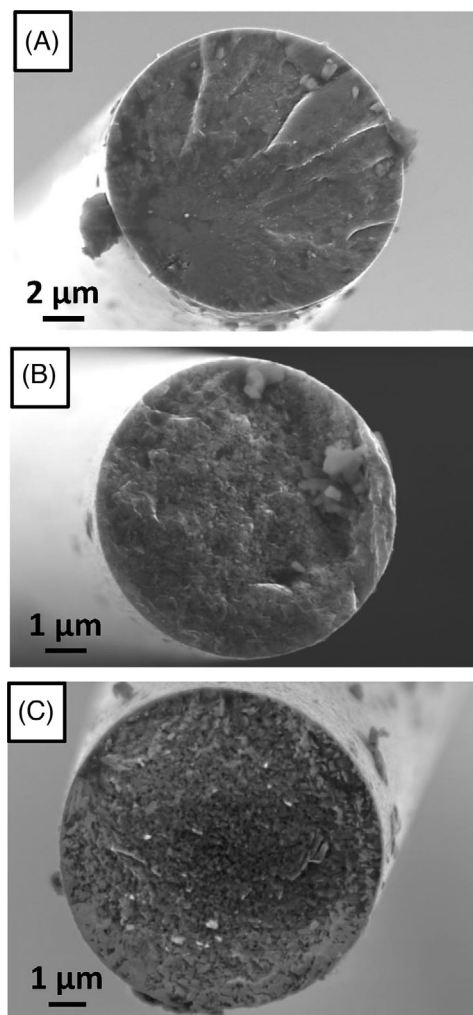


FIGURE 1 Scanning electron microscope (SEM) micrographs of Hi-Nicalon Type S (HNS) (A), Tyranno SA3 (TSA3) (B), and Tyranno SA4 (TSA4) (C) fibers cross-sections.

which was already employed in TSA3 fibers as a sintering agent and to improve the SiC precursor polymer cross-linking,³³ as well as boron but its concentration is significantly higher. However, other impurities concentrations, such as S, Cl, Fe, Ti, Zr, and Hf, were reduced to low levels. The main difference with the HNS fiber lies, on the one hand, in the oxygen concentration, which is really low in TSA4 (62 ppm), in comparison with HNS (4500 ppm) and TSA3 (360 ppm) but, on the other hand, in a nitrogen concentration markedly higher (3200, 110, and 440 ppm, respectively).

The fibers cross-sections observed by SEM are presented in Figure 1. The microstructure of TSA4 fibers (Figure 1C) seems homogeneous, as for the HNS (Figure 1A), even though elongated grains are present, while its grain size seems smaller than TSA3 one (Figure 1B). Moreover, the edge region of the TSA4 also seems more dense, in other words contains less free carbon than its core, even if

this difference between the core and the edge is less pronounced than in SA3 fiber.

3.2 | X-ray photoelectron spectroscopy measurements

XPS surveys are presented in Figure 2. Major peaks of carbon, silicon, and oxygen are detected on each fibers, with additional boron and nitrogen ones (respectively, 190 eV and 398 eV) for the TSA4 fibers.^{12,15} Calcium (≈ 345 eV) is only detected as a trace and should come from the water contamination, either during or after the manufacturing process. Indeed, the sizing is applied in water baths that may not have been completely deionized, leading to trace contamination. Chemical composition of the surface was deduced from the areas of the high-resolution spectra. Depth profiles are presented in Figure 3. As the X-ray source is larger than the fibers diameter (i.e., 200 μm), only a qualitative composition can be obtained in depth.

For each fiber, carbon is the main constituent of the outermost surface. For the HNS and TSA3 fibers, its concentration decreases exponentially with depth, while for TSA4 fibers, it remains constant. On the contrary, the silicon content increases with depth, to reach similar concentrations than C, exhibiting the presence of SiC in the bulk. The most noticeable information on TSA4 fibers is the presence of boron, together with nitrogen at the outermost surface. On the contrary, nitrogen was not detected on the HNS and TSA3 fibers surfaces but its content increases with depth. Remaining nitrogen is detected in the fibers core from precursor filaments spinning under N_2 atmosphere at the beginning of the manufacturing process.⁸ Therefore, the nitrogen concentration is higher than the boron one in TSA4 but their concentrations remain constant after a certain sputtering depth (≈ 350 nm).

After fitting, atomic ratio of the different element and each chemical environments on the outermost surface of each fiber are given in Table 3 and specific spectra of C1s and Si2p are presented in Figures S1 and S2, respectively. SiC is almost undetectable on the HNS fibers surface because of a significant carbon layer, mainly Csp₂, on the contrary to TSA3 and TSA4 fibers, confirming previous results.^{12,15} The amounts of free carbon, in the form of Csp₂ and Csp₃, are also lower on TSA4 fibers since boron nitride (BN) is present.

3.3 | Auger electron spectroscopy

To focus the analysis on a single fiber, AES was performed. The AES depth profiles are presented in Figure 4 on one of the dozen of tested fibers. Only silicon, carbon, and

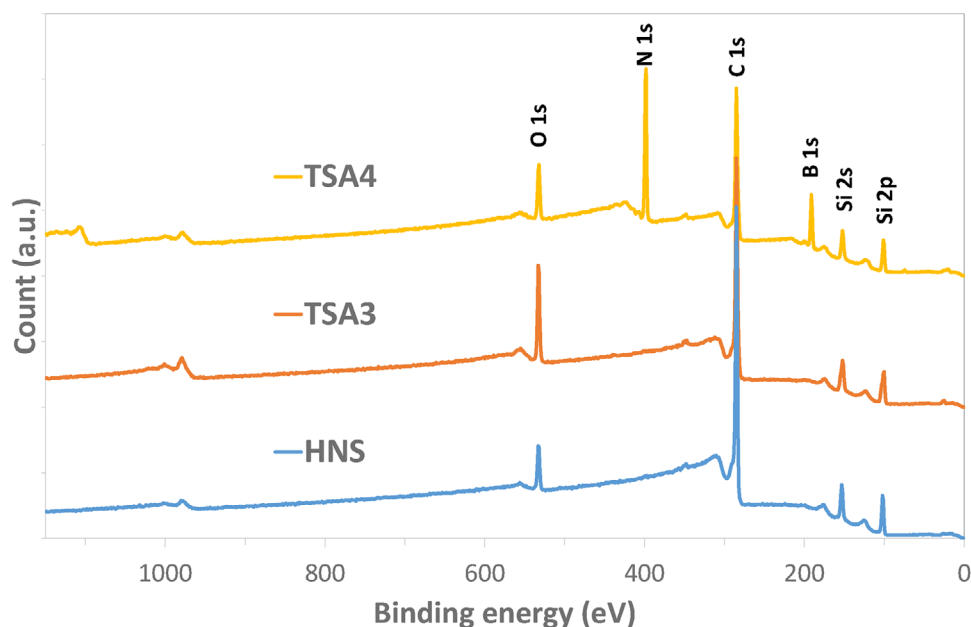


FIGURE 2 X-ray photoelectron spectroscopy (XPS) survey for each fiber.

TABLE 3 Atomic ratio of each element and their chemical environment on the fibers surface.

Element (at%)	HNS	TSA3	TSA4	Bonding (at%)	HNS	TSA3	TSA4
Si	10.8	12.8	8.3	Si-C	4.6	64.8	83.1
				Si-C-O	80.6	7.0	8.4
				Si-O ₂	14.8	28.1	8.4
				Si-C	1.2	10.4	14.6
C	82.3	73.1	40.4	Si-C-O	10.2	3.6	2.5
				Csp ²	53.1	44.0	46.8
				Csp ³	19.1	25.9	24.0
				C-O	7.0	7.9	5.4
				C=O	2.9	2.7	3.0
				O-C=O	2.3	1.8	1.2
				π - π *	4.1	3.7	2.5
Ca	0.4	0.6	0.4	Ca-O	100	100	100
N	0.4	0.2	21.8	N-B	100	100	89.9
				N-B(O)	0.0	0.0	10.1
O	6.0	13.2	6.6	O=C	23.3	22.7	31.8
				O-C, O-Si	55.0	54.5	36.4
				H ₂ O	21.7	22.7	31.8
B	0	0	22.5	B-N	0	0	100

Abbreviations: HNS, Hi-Nicalon Type S; TSA3, Tyranno SA3; TSA4, Tyranno SA4.

oxygen are detected for HNS and TSA3 fibers, with a significant C-rich surface layer before reaching the expected SiC composition (around 30 nm for both fibers). For HNS fibers, the oxygen rate tends to zero in depth, while a higher amount of oxygen is detected on the TSA3 fiber surface, linked to the SiO₂ bonding, previously determined by XPS (Table 3). Moreover, this thin carbon layer can also

correspond to adventitious carbon, coming from hydrocarbons surface contamination. Dong et al.²⁸ showed that the C was in strong excess in comparison with Si (respectively, 60/40 at%) in HNS and that aluminum, a sintering additive of the TSA3 fiber,⁸ was detected. These discrepancies can be attributed to the optimization of the fibers manufacturing process since the early 2000s. The XPS analyses have

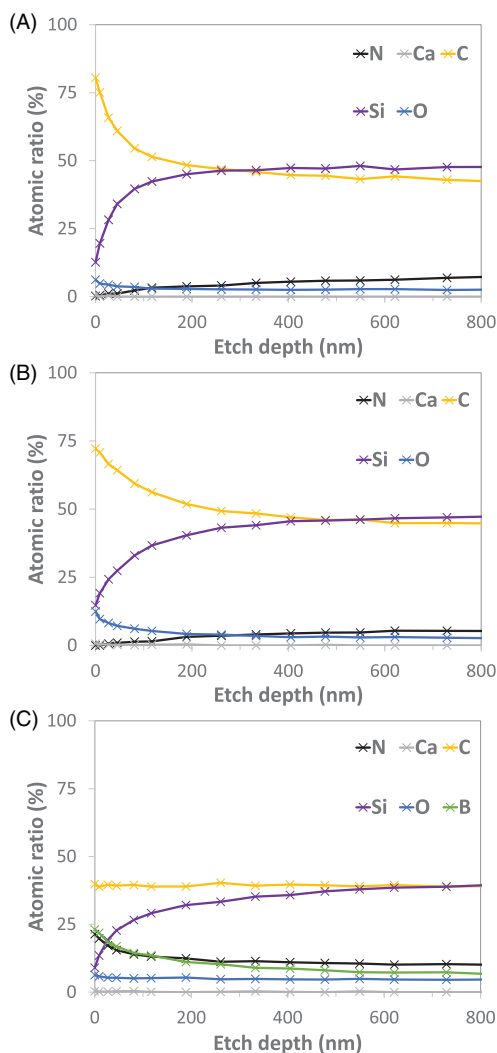


FIGURE 3 X-ray photoelectron spectroscopy (XPS) depth profiles of Hi-Nicalon Type S (HNS) (A), Tyranno SA3 (TSA3) (B), and Tyranno SA4 (TSA4) (C) fibers.

suggested the presence of BN on the TSA4 fibers surface. AES depth profiles focused on one single fiber confirm a ≈ 30 nm rich BN surface layer before reaching the SiC composition (Figure 4C).

3.4 | Transmission electron microscopy

TEM analysis enables to observe the surface of SiC fibers at high resolution (Figure 5A,B). The black layer is the platinum deposit used for FIB etching to protect the surface of the fibers from artifacts linked to ion-matter interactions. The HNS fibers surface exhibits a weakly organized outer carbon layer, approximately ten nanometers thick (Figure 5C). Composed mainly of Csp² and Csp³ carbon bonds, this carbon is found all over the fibers surface and is derived from residues resulting

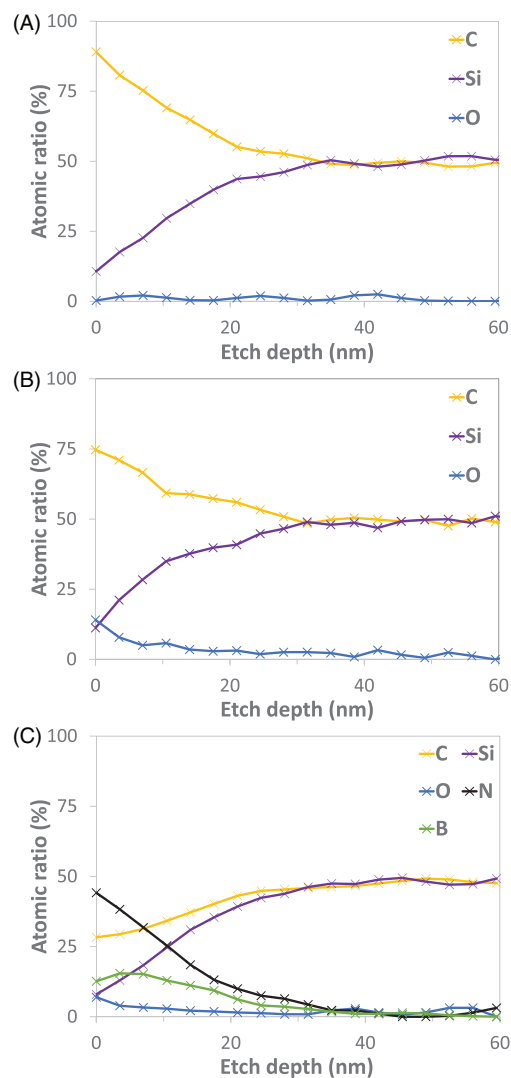


FIGURE 4 Auger electron spectroscopy (AES) depth profiles on Hi-Nicalon Type S (HNS) (A), Tyranno SA3 (TSA3) (B), and Tyranno SA4 (TSA4) (C) fibers.

from pyrolysis of the sizing.¹⁵ The carbon on the surface of TSA3 fibers has been associated with the free carbon growing around SiC grains during fiber processing (Figure 5D). It is highly organized and rich in C–C bonds (Csp²). These stripes of turbostratic carbon are made of ≈ 10 graphene sheets and form a discontinuous layer.

A scheme of the fiber PIPS etching in the longitudinal direction is given Figure 6A and the TSA4 fibers surface in the longitudinal direction is presented in Figure 6B. On the inner side, SiC grains are observed. On the surface, an amorphous layer is noticed, which could come from the amorphization by PIPS etching of the surface. In between these two layers, a highly organized layer is observed by high-resolution transmission electron microscopy (HRTEM). The lattice parameters obtained by

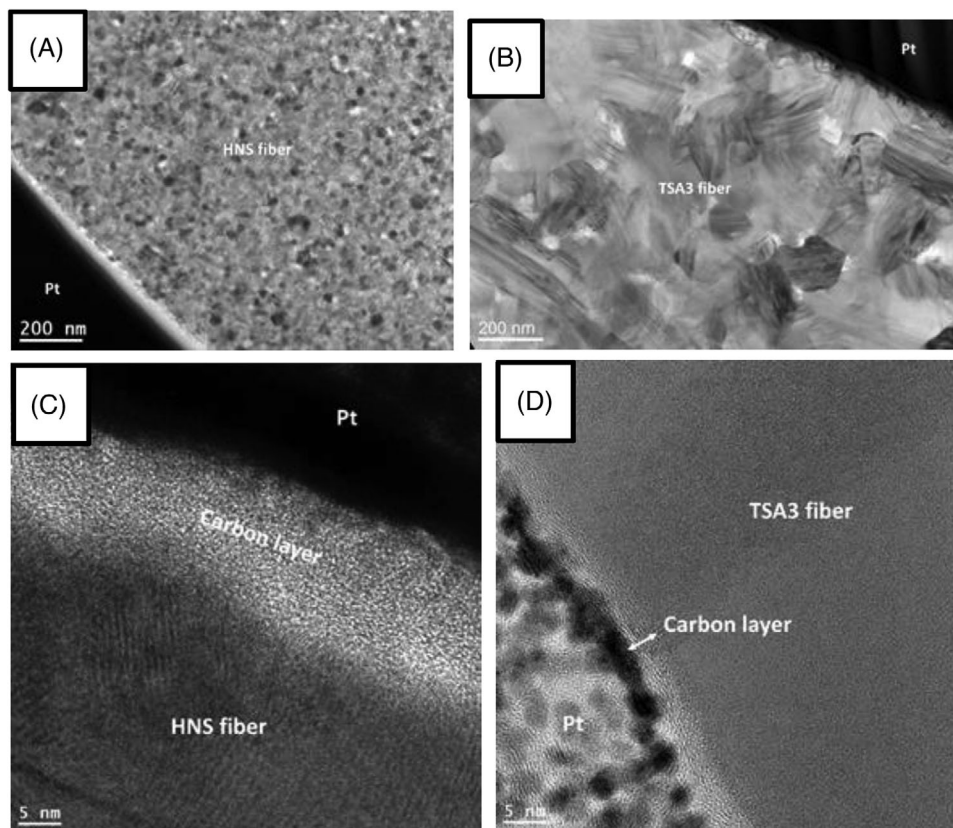


FIGURE 5 Surface of Hi-Nicalon Type S (HNS) fibers (A and C) and Tyranno SA3 (TSA3) fibers (B and D) at different magnifications.

fast Fourier transform (FFT) in this organized region were compared and are estimated to be close to the value of the inter-reticular distance (0.333 nm), deduced from the JCPDS file, for the hexagonal BN. These results confirm the presence of BN on the surface of TSA4 fibers, as identified by AES and XPS. (002) hexagonal BN layers show also in HRTEM image an average stacking sequence close to graphite and tend to fold randomly with thickness.

To avoid amorphization issues, TEM observations were also conducted on the samples prepared by FIB in cross-fiber direction (Figure 7). The black layer on the fibers surface corresponds to the deposited gold to avoid charge effects and the one in surface to tungsten to protect the surface from the ion irradiation during the FIB preparation (as platinum layer in Figure 5). From Figure 7A, it is observed that the SiC grain size of TSA4 and TSA3 fibers are similar, with dimensions ranging from 150 to 450 nm and 200–350 nm, respectively.¹⁴ In addition, a layer about 10 nm thick is observed on the entire surface of TSA4 fibers (Figure 7B). It is difficult at the TEM scale to know if this layer is homogeneous but it covers most of the SiC grains present on the surface of the studied samples. HRTEM images of the near surface of the fibers confirm the results previously obtained and identify the associated FFT to

the presence of a highly organized layer of hexagonal BN (Figure 7C).

Therefore, the presence of an even and homogeneous BN layer on the TSA4 fibers can explain the mechanical behavior of the TSA4-based SiC/SiC composites. Indeed, it was previously observed that HNS/SiC¹⁵ and TSA4/SiC¹⁸ composites without a deposited interphase material already present a pseuductile mechanical behavior. The ultimate tensile strength and strain is however improved with the deposition of an additional pyrocarbon interphase. This thin BN layer ensures adequate bonding between the fiber and the matrix or the additional interphase and deviates the cracks to avoid fibers breakage. Therefore, a parallel can be drawn between the TSA4 fiber and the Sylramic i-BN fiber, forming pseuductile composites,³⁴ presenting a thin (30–100 nm) BN layer synthesized by a high temperature nitrogen heat treatment on a Sylramic fiber.^{35,36}

In comparison with PyC interphases in SiC/SiC composites that are usually thin,^{5,37,38} the BN interphases ranges from 200 nm to few μm . However, the effect of the BN thickness on the mechanical properties of SiC/SiC composites has not clearly been assessed yet. Delpouve et al.³⁹ showed that a more anisotropic BN interphase

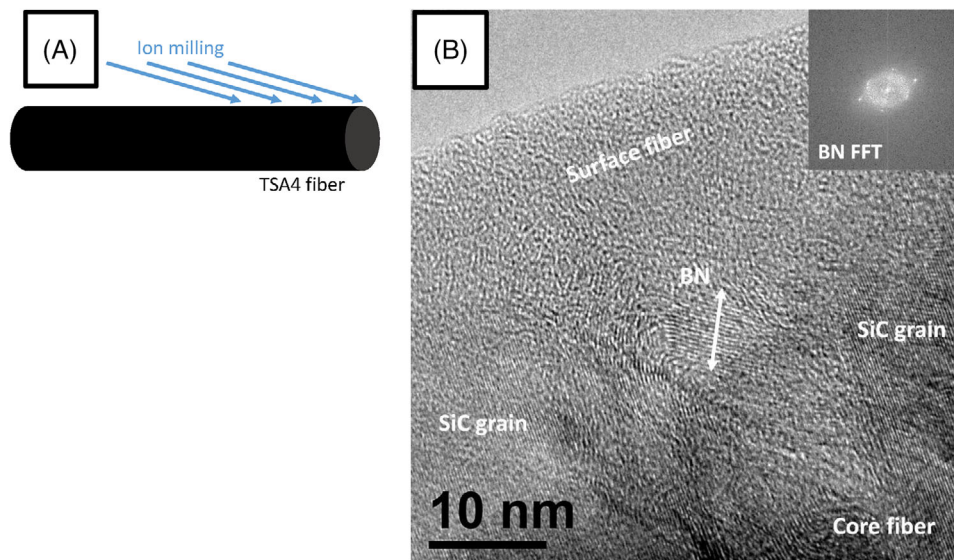


FIGURE 6 Scheme of the precision ion polishing system (PIPS) etching in the longitudinal direction (A) and high-resolution transmission electron microscopy (HRTEM) image of Tyranno SA4 (TSA4) fibers with fast Fourier transform (FFT) pattern of BN layer (B).

confers better mechanical properties but also that thicker (respectively, 500 and 200 nm) interphases leads to better mechanical properties. In HNS/ or TSA3/BN/SiC composites, De Meyere et al.⁴⁰ highlighted that thinner (200 vs. 600 nm) interphases leads to higher shear stresses and more matrix compressive stresses. It was therefore also highlighted that a 500 nm BN interphase leads to higher ultimate tensile strength and Young's modulus than 200 nm, but data are missing on the SiC fibers used (supplied by the Xiamen University).⁴¹ In first generation Nicalon fibers, Norton and Streckert evidenced that the optimum thicker is greater than 0.12 μm but should be lower than 0.55 μm in SiC/BN/Si₃N₄ composites.⁴² Regarding the fibers without a matrix, a layer limited in thickness (90 nm) is better because it heals the fibers flaws and limits the decrease in the mechanical properties because of the interphase lower rigidity.⁴³

In a previous work, the influence of the PyC thickness deposited on the TSA4 fibers on the mechanical behavior was studied.¹⁸ The combination of a PyC interphase with a BN-rich fiber had not been previously studied. The strong dependence of the Young's modulus of the TSA4/SiC composites as a function of the PyC interphase thickness was unexpected. The specific sample geometry, two-dimensional (2D) braided tubes with a $\pm 45^\circ$ angle, does not allow to determine the interfacial shear and friction stresses from the tensile test hysteresis. Recent advances in FIB combined with push out or single cantilever bending³¹ allowed to precisely study the fiber/interphase/matrix bonding and would be suited to determine how cracks interact with this specific type of interphases.

4 | CONCLUSIONS

The different mechanical properties between SiC/SiC composites made of HNS and TSA3 fibers were identified from distinctive chemical composition of the fibers outermost surface. The development and release of a successor of the TSA3 fiber, called TSA4, has aroused interest for ceramic matrix composites manufacturing. Pseudoductile mechanical behavior of the TSA4-based SiC/SiC composites is observed, even without any interphase, suggesting differences in the surface composition. The TSA4 fibers surface was analyzed by XPS, AES, and TEM and compared to the chemical composition of HNS and TSA3 ones. The most noticeable difference was the presence of a thin ($\approx 10\text{--}30$ nm) boron nitride phase on the TSA4 fibers, as a homogeneous and highly crystalized layer, as observed on the Sylramic i-BN fiber. BN is commonly used as an interphase material in ceramic matrix composites, especially in SiC/SiC composites, to confer appropriate fiber/matrix bonding strength and pseudoductility. However, on HNS and TSA3 fibers, differences from early forms of the fibers have been highlighted. Therefore, while searching for optimized process conditions, the fiber producers should keep in mind that small changes in the chemical composition of the fibers outermost surface could lead to strong differences in their mechanical behavior within a fiber/SiC composite.

In comparison with the HNS fibers, the Tyranno fibers present larger grains, which also increase their thermal conductivity and allows their use for applications requiring high thermal conductivity, such as nuclear fuel

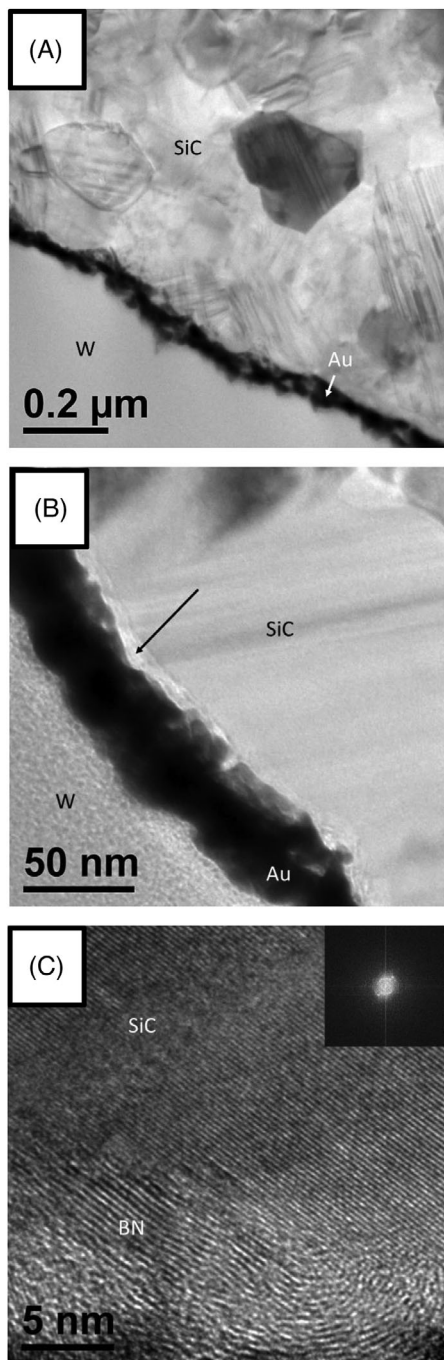


FIGURE 7 Transmission electron microscopy (TEM) (A and B) and high-resolution transmission electron microscopy (HRTEM) (C) images of Tyranno SA4 (TSA4) fibers prepared by focused ion beam (FIB). (Insets) Corresponding fast Fourier transform (FFT) pattern of BN layer in HRTEM image.


cladding material. Boron is usually avoided in cladding materials because of its neutron capture cross-section. Therefore, irradiation experiments are needed to determine the behavior of such a thin layer for nuclear application and if TSA4/SiC composites keep their pseuductility during and after neutron irradiation.

ACKNOWLEDGMENTS

The authors have nothing to report.

ORCID

James Braun  <https://orcid.org/0000-0002-0905-4676>

Mélanie Vaudescal  <https://orcid.org/0009-0009-8150-6890>

REFERENCES

- Nasiri NA, Patra N, Ni N, Jayaseelan DD, Lee WE. Oxidation behaviour of SiC/SiC ceramic matrix composites in air. *J Eur Ceram Soc.* 2016;36(14):3293–302. <https://doi.org/10.1016/j.jeurceramsoc.2016.05.051>
- Zhang M, Chen Q, He Y, Hong Y, Li D, Yang Z, et al. A comparative study on high temperature oxidation behavior of SiC, SiC-BN and SiBCN monoliths. *Corros Sci.* 2021;192:109855. <https://doi.org/10.1016/j.corsci.2021.109855>
- Steibel J. Ceramic matrix composites taking flight at GE aviation. *Am Ceram Soc Bull.* 2019;98:30-33.
- Panakarajupally RP, Kannan M, Morscher GN. Tension-tension fatigue behavior of a melt-infiltrated SiC/SiC ceramic matrix composites in a combustion environment. *J Eur Ceram Soc.* 2021;41:3094–107. <https://doi.org/10.1016/j.jeurceramsoc.2020.10.007>
- Sauder C. Nuclear applications. In: Bansal NP, Lamon J editors. *Ceramic matrix composites.* Hoboken, NJ: John Wiley & Sons, Ltd; 2014. p. 609-646. <https://doi.org/10.1002/9781118832998.ch22>
- Katoh Y. Ceramic matrix composites in fission and fusion energy applications. In: Low IM editor. *Advances in ceramic matrix composites.* Elsevier; 2018. p. 595-622.
- Koyanagi T, Terrani K, Harrison S, Liu J, Katoh Y. Additive manufacturing of silicon carbide for nuclear applications. *J Nucl Mater.* 2021;543:152577. <https://doi.org/10.1016/j.jnucmat.2020.152577>
- Bunsell AR, Piant A. A review of the development of three generations of small diameter silicon carbide fibres. *J Mater Sci.* 2006;41:823–39. <https://doi.org/10.1007/s10853-006-6566-z>
- Wang P, Liu F, Wang H, Li H, Gou Y. A review of third generation SiC fibers and SiCf/SiC composites. *J Mater Sci Technol.* 2019;35:2743–50. <https://doi.org/10.1016/j.jmst.2019.07.020>
- Sha JJ, Hinoki T, Kohyama A. Microstructural characterization and fracture properties of SiC-based fibers annealed at elevated temperatures. *J Mater Sci.* 2007;42:5046–56. <https://doi.org/10.1007/s10853-006-0579-5>
- Havel M, Colombari Ph. Rayleigh and Raman images of the bulk/surface nanostructure of SiC based fibres. *Compos Part B: Eng.* 2004;35:139–47. [https://doi.org/10.1016/S1359-8368\(03\)00086-6](https://doi.org/10.1016/S1359-8368(03)00086-6)
- Buet E, Sauder C, Poissonnet S, Brender P, Gadiou R, Vix-Guterl C. Influence of chemical and physical properties of the last generation of silicon carbide fibres on the mechanical behaviour of SiC/SiC composite. *J Eur Ceram Soc.* 2012;32:547–57. <https://doi.org/10.1016/j.jeurceramsoc.2011.09.023>
- Sha JJ, Nozawa T, Park JS, Katoh Y, Kohyama A. Effect of heat treatment on the tensile strength and creep resistance of advanced SiC fibers. *J Nucl Mater.* 2004;329–333:592–96. <https://doi.org/10.1016/j.jnucmat.2004.04.123>

14. Sauder C, Lamon J. Tensile creep behavior of SiC-based fibers with a low oxygen content. *J Am Ceram Soc.* 2007;90:1146–56. <https://doi.org/10.1111/j.1551-2916.2007.01535.x>
15. Fellah C, Braun J, Sauder C, Sirotti F, Berger M-H. Influence of the carbon interface on the mechanical behavior of SiC/SiC composites. *Compos Part A: Appl Sci Manuf.* 2020;133:105867. <https://doi.org/10.1016/j.compositesa.2020.105867>
16. Buet E, Sauder C, Sornin D, Poissonnet S, Rouzaud J-N, Vix-Guterl C. Influence of surface fibre properties and textural organization of a pyrocarbon interphase on the interfacial shear stress of SiC/SiC minicomposites reinforced with Hi-Nicalon S and Tyranno SA3 fibres. *J Eur Ceram Soc.* 2014;34:179–88. <https://doi.org/10.1016/j.jeurceramsoc.2013.08.027>
17. Oda H, Ishikawa T. Microstructure and mechanical properties of SiC-polycrystalline fiber and new defect-controlling process. *Int J Appl Ceram Technol.* 2017;14:1031–40. <https://doi.org/10.1111/ijac.12719>
18. Braun J, Sauder C. Mechanical behavior of SiC/SiC composites reinforced with new Tyranno SA4 fibers: Effect of interphase thickness and comparison with Tyranno SA3 and Hi-Nicalon S reinforced composites. *J Nucl Mater.* 2022;558:153367. <https://doi.org/10.1016/j.jnucmat.2021.153367>
19. Nakayama Y, Soeda F, Ishitani A. XPS study of the carbon fiber matrix interface. *Carbon.* 1990;28:21–26. [https://doi.org/10.1016/0008-6223\(90\)90088-G](https://doi.org/10.1016/0008-6223(90)90088-G)
20. Gardner SD, Singamsetty CSK, Booth GL, He G-R, Pittman CU. Surface characterization of carbon fibers using angle-resolved XPS and ISS. *Carbon.* 1995;33:587–95. [https://doi.org/10.1016/0008-6223\(94\)00144-O](https://doi.org/10.1016/0008-6223(94)00144-O)
21. Li C, Crosky A. The effect of carbon fabric treatment on delamination of 2D-C/C composites. *Compos Sci Technol.* 2006;66:2633–38. <https://doi.org/10.1016/j.compscitech.2006.03.025>
22. Fellah C, Braun J, Sauder C, Sirotti F, Berger MH. Impact of ex-PAN carbon fibers thermal treatment on the mechanical behavior of C/SiC composites and on the fiber/matrix coupling. *Carbon Trends.* 2021;5:100107. <https://doi.org/10.1016/j.cartre.2021.100107>
23. Lee WH, Lee JG, Reucroft PJ. XPS study of carbon fiber surfaces treated by thermal oxidation in a gas mixture of O₂/(O₂+N₂). *Appl Surf Sci.* 2001;171:136–42. [https://doi.org/10.1016/S0169-4332\(00\)00558-4](https://doi.org/10.1016/S0169-4332(00)00558-4)
24. Severini F, Formaro L, Pegoraro M, Posca L. Chemical modification of carbon fiber surfaces. *Carbon.* 2002;40:735–41. [https://doi.org/10.1016/S0008-6223\(01\)00180-4](https://doi.org/10.1016/S0008-6223(01)00180-4)
25. Dilsiz N, Wightman JP. Surface analysis of unsized and sized carbon fibers. *Carbon.* 1999;37:1105–14. [https://doi.org/10.1016/S0008-6223\(98\)00300-5](https://doi.org/10.1016/S0008-6223(98)00300-5)
26. Ryu S-K, Park B-J, Park S-J. XPS analysis of carbon fiber surfaces—anodized and interfacial effects in fiber–epoxy composites. *J Colloid Interface Sci.* 1999;215:167–69. <https://doi.org/10.1006/jcis.1999.6240>
27. Shen Lu, Tan BJ, Willis WS, Galasso FS, Suib SL. Characterization of dip-coated boron nitride on silicon carbide fibers. *J Am Ceram Soc.* 1994;77:1011–16. <https://doi.org/10.1111/j.1151-2916.1994.tb07260.x>
28. Dong SM, Chollon G, Labrugère C, Lahaye M, Guette A, Brunee JL, et al. Characterization of nearly stoichiometric SiC ceramic fibres. *J Mater Sci.* 2001;36:2371–81. <https://doi.org/10.1023/A:1017988827616>
29. Huang Y, Young RJ. Effect of fibre microstructure upon the modulus of PAN- and pitch-based carbon fibres. *Carbon.* 1995;33:97–107. [https://doi.org/10.1016/0008-6223\(94\)00109-D](https://doi.org/10.1016/0008-6223(94)00109-D)
30. Gouadec G, Colomban P. Non-destructive mechanical characterization of SiC fibers by Raman spectroscopy. *J Eur Ceram Soc.* 2001;21:1249–59. [https://doi.org/10.1016/S0955-2219\(00\)00321-6](https://doi.org/10.1016/S0955-2219(00)00321-6)
31. Gavalda-Diaz O, Manno R, Melro A, Allegrì G, Hallett SR, Vandeperre L, et al. Mode I and mode II interfacial fracture energy of SiC/BN/SiC CMCs. *Acta Mater.* 2021;215:117125. <https://doi.org/10.1016/j.actamat.2021.117125>
32. Fellah C, Lesaint B. Comparative study of ion milling techniques for the preparation of ceramic fibers in transmission electron microscopy. *Micron.* 2024;180:103612. <https://doi.org/10.1016/j.micron.2024.103612>
33. Ishikawa T, Kohtoku Y, Kumagawa K, Yamamura T, Nagasawa T. High-strength alkali-resistant sintered SiC fibre stable to 2,200°C. *Nature.* 1998;391:773–75. <https://doi.org/10.1038/35820>
34. Bhatt RT, Eldridge JJ. Heat treatment effects on microstructure and properties of CVI SiC/SiC composites with Sylramic™-iBN SiC fibers. *J Eur Ceram Soc.* 2023;43:2376–87. <https://doi.org/10.1016/j.jeurceramsoc.2022.12.034>
35. DiCarlo JA, Yun HM. Methods for producing silicon carbide architectural preforms. 2010. US 7.687,016 B1, issued 2010.
36. Bhatt RT, Sola' F, Evans LJ, Rogers RB, Johnson DF. Microstructural, strength, and creep characterization of Sylramic™, Sylramic™-iBN and super Sylramic™-iBN SiC fibers. *J Eur Ceram Soc.* 2021;41:4697–709. <https://doi.org/10.1016/j.jeurceramsoc.2021.03.024>
37. Cao X, Yin X, Fan X, Cheng L, Zhang L. Effect of PyC interphase thickness on mechanical behaviors of SiBC matrix modified C/SiC composites fabricated by reactive melt infiltration. *Carbon.* 2014;77:886–95. <https://doi.org/10.1016/j.carbon.2014.05.092>
38. Ma X, Yin X, Fan X, Cao X, Yang L, Sun X, et al. Improved tensile strength and toughness of dense C/SiC-SiBC with tailored PyC interphase. *J Eur Ceram Soc.* 2019;39:1766–74. <https://doi.org/10.1016/j.jeurceramsoc.2019.01.006>
39. Delpouve H, Camus G, Jouannigot S, Humez B, Plaisantin H, Josse C, et al. Relationship between both thickness and degree of crystallisation of BN interphases and the mechanical behaviour of SiC/SiC composites. *J Mater Sci.* 2022;57:17661–77. <https://doi.org/10.1007/s10853-022-07753-0>
40. De Meyere RMG, Gale L, Harris S, Edmonds IM, Marrow TJ, Armstrong DEJ. Optimizing the fiber push-out method to evaluate interfacial failure in SiC/BN/SiC ceramic matrix composites. *J Am Ceram Soc.* 2021;104:2741–52. <https://doi.org/10.1111/jace.17673>
41. Dai J, Wang Y, Xu Z, Mu R, Liu W, He L. Effect of BN/SiC interfacial coatings on the tensile properties of SiC/SiC minicomposites fabricated by PIP. *Ceram Int.* 2020;46:25058–65. <https://doi.org/10.1016/j.ceramint.2020.06.292>
42. Norton KP, Streckert HH. Effect of BN interfacial coating on the strength of a silicon carbide/silicon nitride composite. *MRS Online Proc Libr (OPL).* 1991;250:239–44. <https://doi.org/10.1557/PROC-250-239>

43. Lv X, Qi Z, Jiang Z, Zhou Y, Zhao W, Jiao J. The microstructure and mechanical properties of silicon carbide fibers with boron nitride interphase. *IOP Conf Ser: Mater Sci Eng.* 2019;678:012061. <https://doi.org/10.1088/1757-899X/678/1/012061>

SUPPORTING INFORMATION

Additional supporting information can be found online in the Supporting Information section at the end of this article.

How to cite this article: Braun J, Fella C, Labrugère C, Vaudescal M, Sauder C. Characterization of the Tyranno SA4 third generation SiC fiber surface and comparison with Tyranno SA3 and HNS fibers. *Int J Appl Ceram Technol.* 2024;e14988.

<https://doi.org/10.1111/ijac.14988>